

Subsurface Probing in Diffusely Scattering Media Using Spatially Offset Raman Spectroscopy

P. MATOUSEK,* I. P. CLARK, E. R. C. DRAPER, M. D. MORRIS,
A. E. GOODSHIP, N. EVERALL, M. TOWRIE, W. F. FINNEY, and A. W. PARKER

Central Laser Facility, CCLRC Rutherford Appleton Laboratory, Didcot, Oxfordshire, OX11 0QX, United Kingdom (P.M., I.P.C., M.T., A.W.P.); Royal Veterinary College, Hawkshead Lane, North Mymms, Hatfield, Hertfordshire AL9 7TA, United Kingdom (E.R.C.D., A.E.G.); Department of Chemistry, University of Michigan, Ann Arbor, Michigan 48109 (M.D.M., W.F.F.); and ICI PLC, Wilton Research Centre, Wilton, Redcar, Cleveland, TS10 4RF, United Kingdom (N.E.)

We describe a simple methodology for the effective retrieval of Raman spectra of subsurface layers in diffusely scattering media. The technique is based on the collection of Raman scattered light from surface regions that are laterally offset away from the excitation laser spot on the sample. The Raman spectra obtained in this way exhibit a variation in relative spectral intensities of the surface and subsurface layers of the sample being investigated. The data set is processed using a multivariate data analysis to yield pure Raman spectra of the individual sample layers, providing a method for the effective elimination of surface Raman scatter. The methodology is applicable to the retrieval of pure Raman spectra from depths well in excess of those accessible with conventional confocal microscopy. In this first feasibility study we have differentiated between surface and subsurface Raman signals within a diffusely scattering sample composed of two layers: *trans*-stilbene powder beneath a 1 mm thick over-layer of PMMA (poly(methyl methacrylate)) powder. The improvement in contrast of the subsurface *trans*-stilbene layer without numerical processing was 19 times. The potential applications include biomedical subsurface probing of specific tissues through different overlying tissues such as assessment of bone quality through skin, providing an effective noninvasive means of screening for bone degeneration, other skeletal disease diagnosis, and dermatology studies, as well as materials and catalyst research.

Index Headings: Raman spectroscopy; Confocal microscopy; Diffuse scattering; Turbid media; Photon migration; Optical tomography.

INTRODUCTION

Diffusely scattering media are frequently encountered in many analytical applications: examples include monitoring of food products, colloids, polymers, catalysts, powders in general, coating technology, dermatology applications involving the probing of tissue, and biochemical identification for medical studies and treatments. Such samples are often highly heterogeneous and can be made of various layers, each having a different chemical make-up. A major goal for analytical science is to provide a method capable of determining the chemical composition of subsurface layers in turbid media in a non-destructive way. The benefits of this can be illustrated

using the example of noninvasive Raman probing of bones¹ where signal quality from bone is crucial in order to provide an accurate and correct diagnosis as to whether a disease is present. Conventional Raman signatures of bone collagen are masked by undesired Raman signals from overlaying tissue containing similar collagenous proteins. Thus, the separation of the two collagen-specific Raman spectral components from the surface and subsurface would be highly desirable for improved sensitivity and, ultimately, disease diagnosis. This task is, however, hugely complicated due to the inability to form sharp optical images from within turbid media by conventional optical methods such as confocal microscopy, which is only applicable typically to depths on the order of the transport length of the scattering medium.² The transport length describes the average distance photons travel before deviating significantly from their original direction of propagation and it is typically an order of magnitude higher than the mean free scattering length (i.e., the average distance between scattering events) of photons in the medium.

Recently, we reported an effective method for the recovery of subsurface Raman signals in diffusely scattering media from depths in excess of the transport length, using ultrafast temporal gating.³⁻⁵ These studies built upon earlier work of others on both elastically and non-elastically scattered light.^{4,6,7} For the ultrafast temporal gating investigations we used a tunable, 1 ps, 1 kHz laser, with an optical Kerr gate opening for 4 ps to permit the detection of Raman photons scattering from solid or liquid samples. Using an optical delay line, the time delay between the laser pulse illuminating the sample and collection of the Raman signal can be varied. Using this arrangement we investigated a two-layer sample composed of *trans*-stilbene powder covered by a 1 mm thick layer of PMMA (poly(methyl methacrylate)) powder. The work demonstrated how, by using temporal gating of the Raman signals, the signal contrast of the sub-*trans*-stilbene can be improved by a factor ≥ 5 by rejecting the Raman signal from the PMMA overlayer. The temporal gating concept has several inherent advantages, the major

Received 21 December; accepted 11 January 2005.

* Author to whom correspondence should be sent.

one being that it has the ability to suppress fluorescence.^{8,9} It is also extremely effective for specifically collecting Raman spectra from the uppermost surface layer by rejecting the time-delayed Raman scattering coming from the lower layer. In other words, one can optimize detection of either the surface or subsurface Raman signals simply by varying the time delay, making it very suitable for depth-profiling a variety of opaque, stratified materials.

Despite the Kerr gate's effectiveness, the wider applicability of this technique is hindered by the inherent instrumental complexity, as well as a requirement for the use of relatively high intensity laser pulses. Not only does this pose practical difficulties, it also raises potential safety problems in biomedical applications such as bone studies and the probing of human tissue in cancer, due to the high peak powers of the laser, which operates above the maximum permitted exposure limits of laser radiation. Here we present a novel and more simple approach, enabling the retrieval of deep-layer Raman signals and their separation from those of the overlaying matrix. Apart from being substantially less complex in terms of instrumentation, it is also compatible with the use of lower power continuous wave (cw) laser beams, alleviating the above-mentioned safety issues. The technique also lends itself to use with customized optical fiber arrays, making it well suited for remote monitoring, e.g., in industrial processes or in intra-cavity probing in medical applications.

The proposed methodology is based on the collection of Raman spectra from regions spatially offset, by different amounts, from the point of incidence of the probe laser beam on the surface of a diffusely scattering sample (see Fig. 1a). Crucially, such an array of spectra contains different relative Raman contributions from the surface and subsurface layers. This is the key effect on which this technique is based. As the collection point is moved away from the probe launch point, the contribution of the spectrum from the top layer diminishes much faster than that from deeper layers, because Raman photons that are generated deeper within the sample are more likely to migrate laterally before they are emitted from the sample surface. By collecting a set of spectra at different distances from the launch point and processing them using a multivariate data analysis technique, one can extract approximations to the pure Raman spectra of the individual layers. The proposed technique is akin to optical tomography using near-infrared (NIR) absorbance spectroscopy, which has been widely used in the past, for example, in functional imaging of the brain.¹⁰

The variation in the relative content of Raman signals from different layers with the spatial offset originates from the random properties of the photon migration effect. The migrating photons in essence undergo a 'random walk' within the medium and their direction is randomized about every transport length along the propagation distance.⁶ When a Raman signal is collected from the surface of a sample at the point of probe beam incidence, the spectrum contains a relatively large signal contribution from the top layer due to the highest probe photon density at this point. With increasing sample depth this intensity quickly diminishes as the light intensity is progressively diluted through the photon diffusion pro-

cess. The scattered Raman light propagating back to the surface is subject to the same diffusion process, and this leads to further dilution of its intensity as measured at the point of incidence of the probe beam. This effect results in a substantially larger proportion of Raman photons detected from the surface layer than those from deeper layers compared to optically transparent media probed in the same geometry. Raman photons that are generated deep below the surface are less likely to migrate back to exactly the point of incidence of the probe beam compared with those that were generated at the surface and near the point of incidence.

When collecting Raman light from a point laterally offset from the point of probe beam incidence, the probe light intensity within the sample becomes more equally distributed along its depth. This is because the probe light first has to propagate sideways through the medium from the incidence point to this area and is randomized on its path through photon diffusion. Consequently, the emitted Raman signal detected at the surface at this point contains a higher proportion of the deeper layer signal than that in the spectrum collected with no lateral offset. In conventional Raman spectroscopy, only signal from the probe launch point and its vicinity would usually be collected and averaged to a single spectrum. This results in a higher relative signal from the top layer being present in the collected spectrum, compared with the proposed offset collection geometry.

The proposed technique can be deployed in two possible basic geometries: (1) point collection and (2) collection from the circumference of (multiple) concentric circles symmetrically centered on the probe beam incidence point (see Fig. 1b). The point-like collection geometry represents the simplest adoption of this concept. The concentric circle geometry is, however, superior as it yields much higher collection efficiency, but it requires the use of optical fibers to image the individual circles at different positions on the spectrometer slit. This enables their imaging, after wavelength dispersion, as separate horizontal strips, on a charge-coupled device (CCD) camera, with the vertical position corresponding to an offset distance on the sample surface.

The spatially offset Raman spectroscopy (SORS) approach is well suited to the suppression of surface Raman signals and retrieving pure Raman spectra of deeper layers. This is demonstrated on a two-layer sample chosen to be identical to that used in our earlier temporal Kerr gating work,³ namely a 1 mm thick PMMA powder layer covering a *trans*-stilbene powder layer. This choice enables a direct comparison between the two techniques to be made. A small difference in probe wavelengths, 514 nm as opposed to 400 nm used in the temporal Kerr gating study, represents only a negligible difference in the experimental conditions, since the properties of diffuse scattering are not strongly dependent on wavelength in the regime where the wavelength of light is much smaller than the particle size of the medium.⁶

EXPERIMENTAL

A schematic diagram of the laser and the Raman detection apparatus is shown in Fig. 2. The probe wavelength was the 514 nm output from a cw argon ion laser

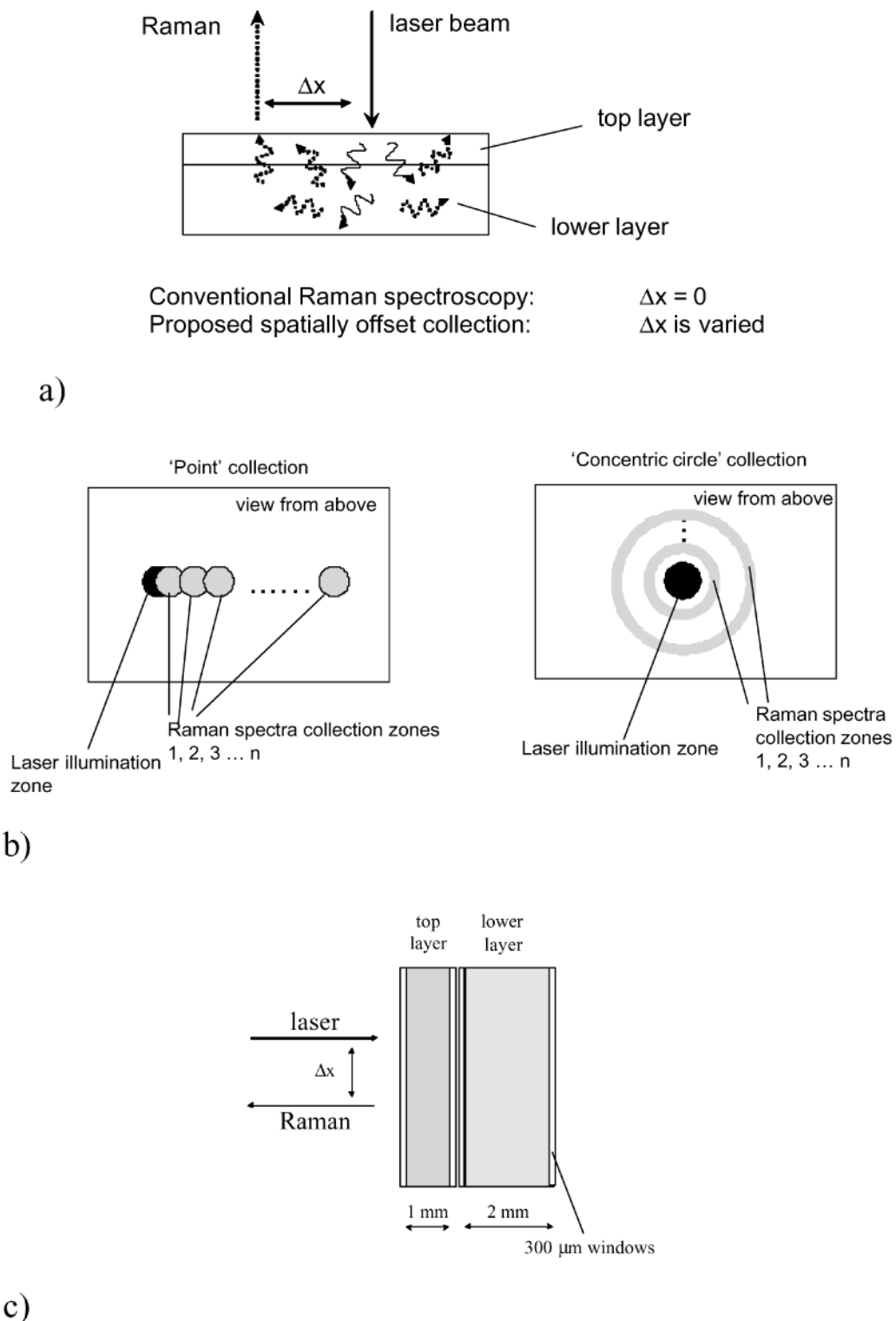


FIG. 1. (a) The principle of spatially offset Raman spectroscopy. (b) Two principal collection geometry configurations. (c) Two-layer sample geometry used in the experiments.

(Coherent Innova 90-5 UV), with a power of 12 mW at the sample. The laser plasma lines were removed using a Pellen–Brocca prism. The laser beam was focused to a diameter of 300 μm using a 1 m focal length lens, and launched into the sample at normal incidence. The Raman light was collected in backscattering geometry using a 50 mm diameter, $f/1$ collection lens, and imaged onto

the spectrometer slit with a magnification of 2.5. The Raman light was dispersed using a conventional three-stage imaging spectrometer (Spex Triplemate 1877 Series with $f/\# = 6.3$) and imaged onto a CCD camera (Andor Technology, DU420-BU2 (250 nm), with 1024 \times 255 active pixels, size 26 \times 26 μm). The CCD quantum efficiency in the wavelength region of the Raman spectra

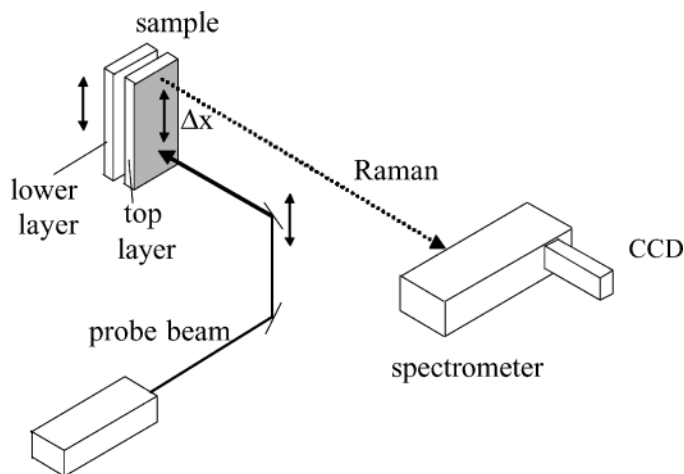


FIG. 2. Schematic diagram of the experimental setup.

was 65%. The spectrometer final stage slit width was set to 120 μm . The CCD camera was binned vertically across 20 pixels to maintain spatial selectivity.

The sample was mounted on an x - y - z micro-positioning stage and moved vertically, together with the last turning prism (6 \times 6 mm, quartz) placed right in front of the collection lens (see Fig. 2), which reflects the probe beam arriving from below onto the sample, keeping the point of incidence on the sample fixed with respect to the sample. In this configuration, the spectrograph was always collecting light from a fixed region in space and the sample was scanned across this imaging zone, the pump beam incidence point remaining fixed on the sample surface.

The test sample consisted of two layers. The first layer was a 1 mm optical path cuvette of 1 cm width and \sim 4 cm height, with 300 μm custom-made fused silica front and back windows, filled with PMMA (poly(methyl methacrylate)) spheres of \sim 20 μm diameter (see Fig. 1c). The spheres were loosely packed in the cell, using mechanical tapping during filling to eliminate voids. This layer was followed by another cell of 2 mm optical path filled with *trans*-stilbene fine powder that was ground using a pestle and mortar. The use of cuvettes was to provide a simple method of sample handling and thickness control, although this generates weak Raman features due to the wall material. The laser beam was first incident on the PMMA layer. The spatially offset Raman spectra (SORS) were collected using the point collection geometry described in Fig. 1b.

The multivariate analysis of the Raman data set was performed using a variant of principal component analysis (PCA), namely band target entropy minimization (BTEM).^{11–14} This method was first introduced by Garland and later adapted by one of us.¹⁵ BTEM provides several advantages over other PCA based automated factor recovery algorithms. The first is that BTEM can rotate and recover small amounts of the targeted factor from many more higher-noise eigenvectors than other methods. This enhances the ability of BTEM to recover factors from trace components. BTEM also provides recovered factors with higher signal-to-noise ratios than other multivariate data reduction methods. BTEM is fast and does

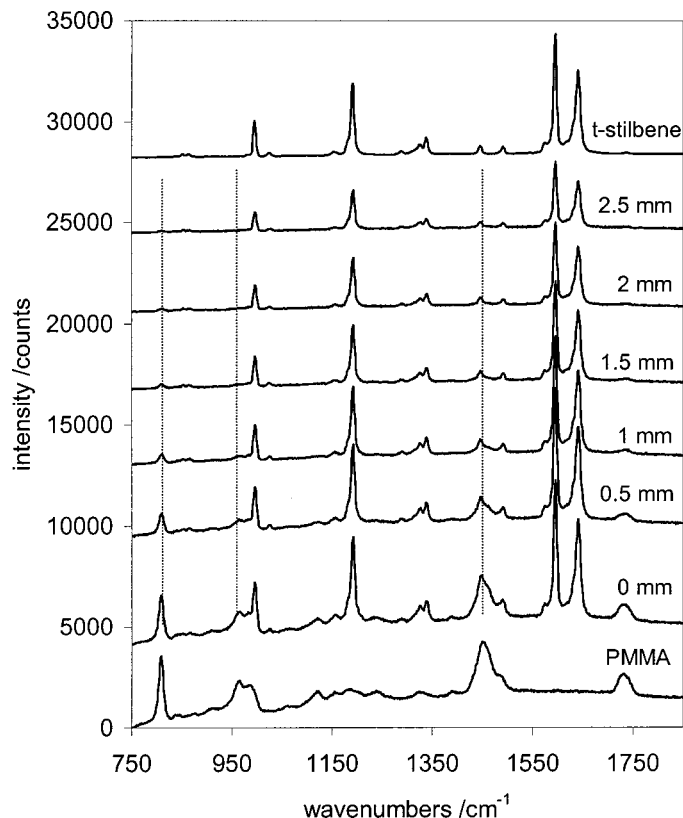


FIG. 3. A set of spatially offset Raman spectra collected from a two-layer system consisting of a 1 mm layer of PMMA spheres followed by a 2 mm layer of *trans*-stilbene powder measured using the 514 nm probe wavelength. The SORS spectra are shown for different spatial offsets, Δx , between the Raman collection and the probe beam incidence points on the sample surface indicated next to each spectrum. The top and bottom spectra are those of pure *trans*-stilbene and pure PMMA layers, respectively, obtained in separate measurements. The spectra are offset for clarity. The acquisition time was 100 s for each spectrum. Note the line markers are for guidance of the eye to demonstrate the changing relative intensity of the PMMA bands with the spatial offset.

not require an *a priori* knowledge of the system composition.

The SORS spectra were imported into Matlab R11 (The Mathworks Inc., Natick, MA) and processed with both built-in and locally written scripts. The ten largest eigenvectors generated after performing a singular value decomposition on the original data set were included in the BTEM rotation. Pure spectra of PMMA and *trans*-stilbene were not included in this dataset and no baseline correction was performed.

RESULTS

A set of Raman spectra measured with a varying degree of spatial offset Δx is shown in Fig. 3. The measurement was performed on the two-layer system, 1 mm PMMA powder on top of 2 mm *trans*-stilbene powder. For comparison, the Raman spectra of the pure layers measured in separate experiments are also displayed. The top spectrum in Fig. 3 is that of pure *trans*-stilbene and the bottom one is that of pure PMMA. The spectrum measured with zero offset represents the Raman spectrum one would typically obtain using a conventional Raman instrument. It is evident that it contains an appreciable contribution from the top layer. The gradual separation

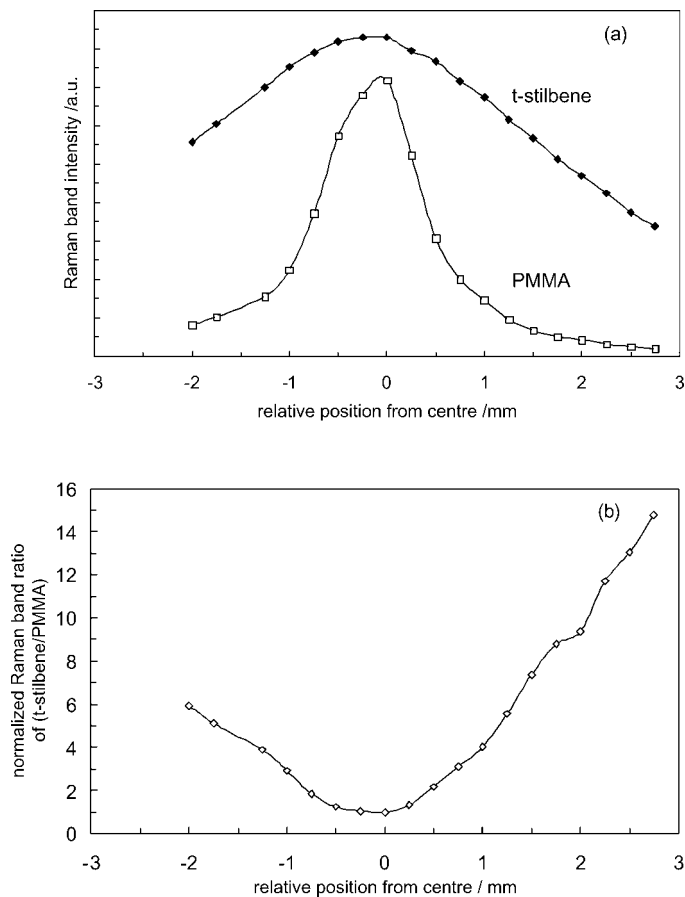


FIG. 4. (a) Intensity plots for PMMA and *trans*-stilbene Raman spectra and (b) the Raman intensity ratio (*trans*-stilbene/PMMA) of the spectra presented in Fig. 3 as a function of the spatial offset between the Raman collection and laser beam incidence points.

of the PMMA and *trans*-stilbene signals is clearly accomplished using the SORS approach as one keeps increasing the lateral offset between the Raman collection point and the point of probe beam incidence, and is clearly observable in the raw data set presented. This is because as the offset distance is increased the signal intensity of the surface PMMA layer drops more than that of the lower layer, as predicted. At distances of >2 mm one reaches around an order of magnitude improvement in the ratio of the lower layer to the top layer Raman signals. It should be pointed out that although it is relatively easy to eliminate the signal due to PMMA simply by increasing Δx , it is not possible to obtain a pure PMMA spectrum in raw spectra, because the Raman scatter from stilbene is so strong it dominates even when $\Delta x = 0$, unlike in the temporal Kerr gating approach where the suppression of the lower layer signal is straightforward and highly effective.³

Figure 4a shows the dependence of the absolute Raman intensities of the individual spectra on the spatial offset. The data were obtained by numerical curve fitting of several intense *trans*-stilbene bands at 1575, 1595, 1632, and 1641 cm^{-1} , and bands at around 809, 1455, and 1728 cm^{-1} for PMMA. The plot clearly demonstrates that as the Raman collection point is moved away from the probe illumination zone, i.e., the spatial offset, Δx , is increased, the Raman signal from the bottom layer dimin-

ishes much more slowly than that from the top layer. This results in the overall relative Raman intensity ratio of the bottom over the top layer improving with the increased spatial offset, as shown in Fig. 4b. The ratio is practically independent of the sign of the offset and dependent only on its magnitude, as is expected as the layers are each of uniform thickness and character.

To quantify the contrast improvement achievable on this sample by this approach, we have acquired a Raman spectrum with a longer acquisition time (1000 s) at an offset of 3.5 mm. Figure 5a shows this spectrum, along with a Raman spectrum acquired with zero offset, scaled to the same height as the *trans*-stilbene bands. By subtracting the pure *trans*-stilbene spectrum from these spectra we obtained the residual PMMA contributions within the individual spectra (see Fig. 5b). By analyzing the intensity of the residual PMMA component we established that the contrast of the lower layer has been improved by a factor of 19 by rejecting the top layer spectral component. This result compares extremely favorably with the contrast improvement obtained using the temporal gating in our earlier work,³ where the attained contrast improvement was a factor of 5 (although this figure was noise limited). Another striking observation is that the signal-to-noise ratio obtained using the much more simple spatial gating approach was substantially higher than that observed with the temporal gating approach. This is understandable as the spatial gating technique integrates all Raman components spread in the temporal domain, unlike in the temporal approach where the ultrafast gating results in a severe reduction of the collectable light, as discussed in our earlier work.³

The total attenuation of the Raman *trans*-stilbene signal by the 1 mm PMMA layer was measured to be around 80 by comparing Raman signal strengths of the *trans*-stilbene layer with and without the PMMA overlayer with the zero offset. This loss of signal through the diffusion process, inevitably also present in conventional Raman spectroscopy, can, however, be effectively offset through further refinements in the collection efficiency, for example, by adopting the circular collection geometry shown in Fig. 1b or by using a lower f-number and higher throughput spectrograph.

In a situation where one desires a better resolution of surface and subsurface Raman signals than is achievable directly within the raw spectra obtained by offsetting the collection and probe launch points, a multivariate data analysis procedure can be effectively deployed. For this approach to be applicable, a set of Raman spectra measured at various offsets is required. To achieve an effective numerical decomposition, the number of spectra within the set should ideally be at least an order of magnitude higher than the number of layers present in the sample. The data collected by SORS is particularly amenable to multivariate data analysis. Multivariate data reduction techniques provide an advantage when one desires a complete separation of the spectral features of the surface and subsurface layers. These methods also provide a means of separating spectral features from layers that may have a moderate to high degree of spectral overlap, or where contributions of individual components to spectral band envelopes may not be known because spec-

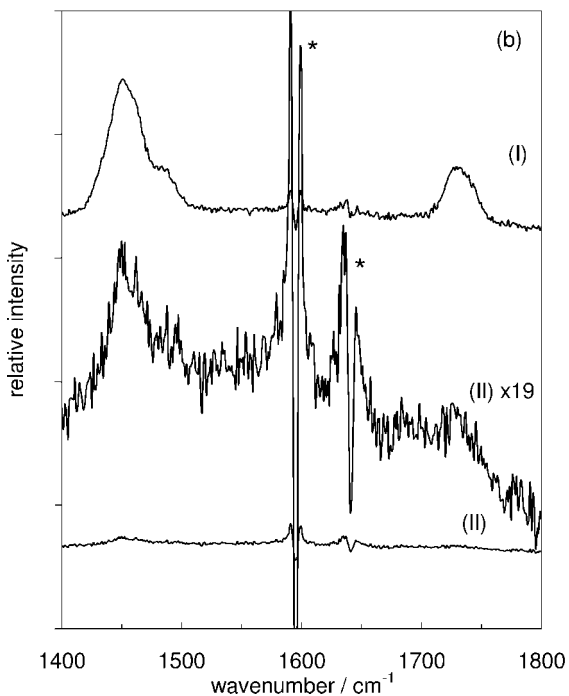
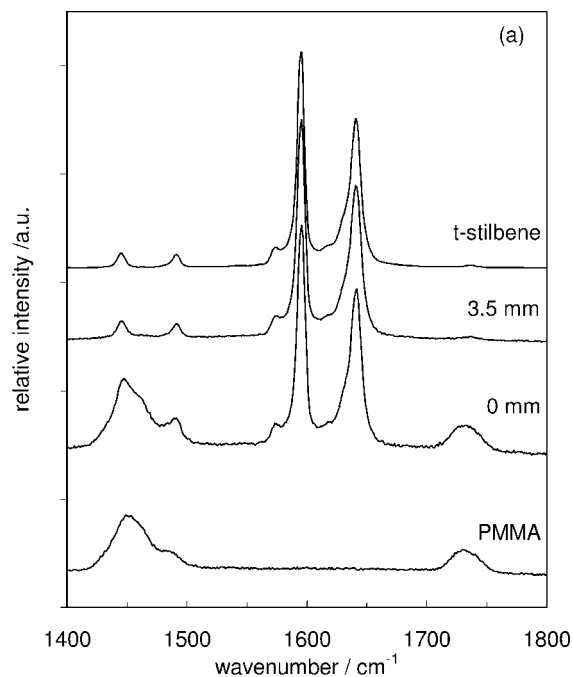


FIG. 5. (a) The zero and 3.5 mm spatially offset Raman spectra measured using a probe wavelength of 514 nm on a two-layer system consisting of a 1 mm thick layer of PMMA spheres followed by *trans*-stilbene powder. The top and bottom spectra are those of pure *trans*-stilbene and pure PMMA layers, respectively, obtained in separate measurements. The spectra are offset for clarity. (b) Residual Raman signals of the PMMA layer present in individual SORS spectra shown in (a) with pure *trans*-stilbene spectra subtracted indicating the 19 \times reduction in the PMMA Raman component in terms of its relative content upon the introduction of a 3.5 mm spatial offset. (I) and (II) The 0 and 3.5 mm spectra, respectively. The symbol (*) denotes subtraction artifacts.

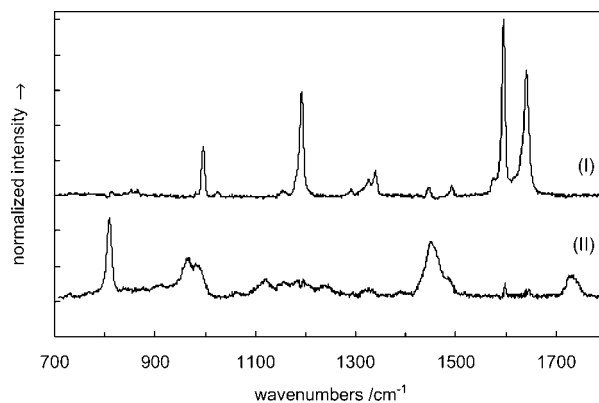


FIG. 6. The result of band target entropy minimization (BTEM) analysis applied to the full data set represented in Fig. 3. The spectra were 'blind' decomposed into individual components: (I) *trans*-stilbene and (II) PMMA.

tra of the pure components may not be obtainable or known.

The recovered factors from the BTEM analysis using 20 spectra are shown in Fig. 6. An approximate factor for pure *trans*-stilbene was recovered by targeting the approximately 1595 cm^{-1} band and an approximate factor for pure PMMA was recovered by targeting the approximately 809 cm^{-1} band. These factors are excellent approximations to the pure spectra, although weak residual features due to *trans*-stilbene can be seen in the PMMA factor near 1600 and 1650 cm^{-1} (Fig. 6). A higher number of SORS spectra provided in the BTEM procedure would be expected to provide a still higher degree of separation. A luminescence background factor was constructed from one of the original input spectra using an iterative polynomial fitting algorithm¹⁶ typically used for baseline correction. In this case 100 fitting cycles using a third-order polynomial were used to generate the baseline. These three factors were then used to reconstruct the dataset with less than 3% error.

The described spatial 'gating' methodology, in combination with BTEM, thus offers an extremely powerful yet simple methodology for extracting virtually pure Raman signals from individual layers within diffusely scattering media. The probed sample depths can be well in excess of the transport length, which sets a depth limit on conventional confocal Raman microscopy. In our case, the transport length of the medium was estimated to be 200 μm . Importantly, the entire process can be performed 'blind', i.e., without any prior knowledge of the chemical constituents of the layers. The technique thus has ideal prerequisites for sensitive subsurface probing of diffusely scattering materials such as tissue in a noninvasive way for the purposes of disease diagnoses.

In cases where the sample is known to consist of only two layers of different composition (if this is not known, then estimates of the number of distinct components can often be obtained directly from simple PCA), an even simpler methodology can be used to extract the pure signals of individual layers. This case is possible when the two spectra of the two components contain an identifiable band, or bands, that are not overlapped. In this situation, a simple scaled subtraction can be used to separate the spectra of the individual layers from each other. In the

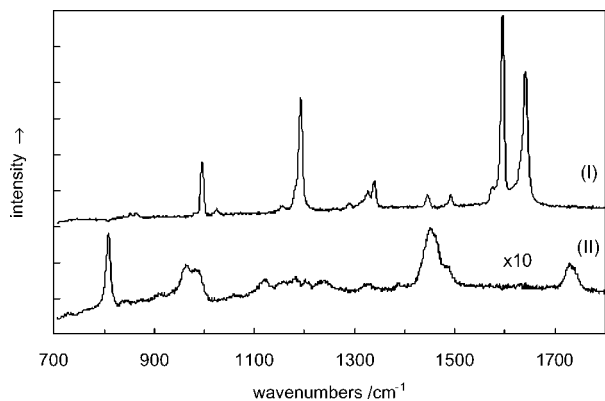


FIG. 7. The result of a simple scaled subtraction of Raman spectra obtained with the zero and 2 mm offset. The true decomposition in this simple way is achieved on the basis of the knowledge that the system contains *two* layers and the Raman spectra from individual layers have a non-overlapping region: (I) *trans*-stilbene and (II) PMMA.

process, one Raman component is eliminated by a scaled subtraction of two spectra measured with two different spatial offsets, canceling out one or the other spectral component in the process. The results of this simple extraction procedure are shown in Fig. 7. The spectra used in this analysis were measured with zero and 2 mm offsets. The result is clearly satisfactory; in fact, the PMMA spectral estimate is superior to that obtained with BTEM (no residual bands due to *trans*-stilbene are observed). However, its applicability is limited since it requires the above conditions to be satisfied, in contrast to the PCA/BTEM analysis, which works without prior knowledge of numbers of components or assignment of bands, and in the absence of any pure spectral bands. Also, BTEM analysis can, in principle, handle large numbers of components provided SORS spectra are available for a sufficiently large number of offsets.

The exact degree of the 'suppression' or separation of two layers in general situations depends on a variety of parameters. These are the thickness of the top layer, that of underlying matrix, the probe beam diameter, the exact collection geometry (i.e., the offset length and the size of the collection aperture), the wavelength of the probe light used, the absorption coefficients of each layer at the laser and Raman wavelengths, and the transport length of the medium. For the technique to be effective, the beam diameter and collection aperture should preferably be smaller than the thickness of the top layer. In general terms, a better spectral separation of the two components is likely to be achievable for thinner top layers and thicker underlying matrixes. The reason for this is that migrating probe photons are quickly lost from the thin top layer, either downwards to the lower layer, or upwards through the air-sample interface. On the contrary, probe photons penetrating into the thick underlying matrix will migrate for prolonged periods of time, generating a much larger number of Raman photons than those within the thin surface layer. (The probability of generation of a Raman photon is proportional to the survival time of a probe photon.⁵) Probe photons within a very thick lower layer can only undergo loss through the upper interface, assuming no absorption is present. We have previously

shown how this mechanism allows us to easily reject the signals from thin surface layers using temporal gating.³

In previous work, we have shown that, in the absence of photon absorption, the Raman photon survival times can exceed 1 nanosecond in fine powders.⁴ In effect, the probe photons launched into tissue such as bone are locked within it, forming a very effective generator of Raman photons if no absorption is present. As a result of this, a many orders of magnitude higher number of Raman photons can be generated within diffusely scattering medium compared to an equivalent system that is optically transparent and that quickly loses photons through its boundaries. However, any degree of absorption of the probe or Raman photons will lead to the fast loss of photons, diminishing the overall yield of Raman signal. Therefore, for the SORS to be effective, it is essential that the measurements be performed at wavelengths as free as possible from absorption. In living tissue this condition can be satisfied outside the hemoglobin absorption region in the NIR¹⁰ (~800 nm). Although the melanin absorption spectrum continues further into the near-infrared region, attenuation of laser light is dominated by light scattering rather than by absorption in this region.¹⁷

The discussion so far has only dealt with methods for obtaining pure spectra of stratified components. However, computation of the *depth* of the component layers is equally important for understanding the structure of a stratified material. Our previous work has shown how Monte Carlo modeling can be used to relate the observation time to the average depth of generation of a Raman photon.⁵ This same model can, in principle, also be used to compute the average radial offset for a Raman photon as a function of its generation depth, and hence the expected variation in spectral contrast ratio. We will return to this topic in a future paper.

CONCLUSION

We have proposed and demonstrated a simple noninvasive methodology for the extraction of Raman spectra from a deep layer within a diffusely scattering sample. The method is based on collecting a set of Raman spectra from laterally offset collection points away from the point of probe beam launch, which we refer to as spatially offset Raman spectroscopy (SORS). In combination with multivariate data analysis, the technique can be used for the effective extraction of almost pure Raman spectra of top and underlying layers, without any prior knowledge of their chemical composition. The technique was demonstrated to be capable of separating a lower layer Raman signal from that of an overlying matrix. The technique holds great promise for biomedical applications, where monitoring subsurface tissue layers normally would require sectioning the superficial tissues, or many analytical applications such as catalysts, food, polymer research, and dermatology applications.

ACKNOWLEDGMENT

We wish to thank Dr. Darren Andrews of CCLRC for his support of this work and the financial contribution of CLIK Proof-of-Concept Fund for enabling this study. M.M. acknowledges the support of the University of Michigan Bone Research Center through NIH grant P30 AR46024.

1. A. Carden and M. D. Morris, *J. Biomed. Opt.* **5**, 259 (2000).
2. C. J. H. Brenan and I. W. Hunter, *J. Raman Spectrosc.* **27**, 561 (1996).
3. P. Matousek, N. Everall, M. Towrie, and A. W. Parker, *Appl. Spectrosc.* **59**, 300 (2005).
4. N. Everall, T. Hahn, P. Matousek, A. W. Parker, and M. Towrie, *Appl. Spectrosc.* **55**, 1701 (2001).
5. N. Everall, T. Hahn, P. Matousek, A. W. Parker, and M. Towrie, *Appl. Spectrosc.* **58**, 591 (2004).
6. B. B. Das, F. Liu, and R. R. Alfano, *Rep. Prog. Phys.* **60**, 227 (1997).
7. J. Wu, Y. Wang, L. Perelman, I. Itzkan, R. R. Dasari, and M. S. Feld, *Appl. Opt.* **34**, 3425 (1995).
8. P. Matousek, M. Towrie, A. Stanley, and A. W. Parker, *Appl. Spectrosc.* **53**, 1485 (1999).
9. P. Matousek, M. Towrie, C. Ma, W. M. Kwok, D. Phillips, W. T. Toner, and A. W. Parker, *J. Raman Spectrosc.* **32**, 983 (2001).
10. H. Koizumi, Y. Yamashita, A. Maki, T. Yamamoto, Y. Ito, H. Itagaki, and R. Kennan, *J. Biomed. Opt.* **4**, 403 (1999).
11. E. Widjaja, C. Z. Li, and M. Garland, *Organometallics* **21**, 1991 (2002).
12. W. Chew, E. Widjaja, and M. Garland, *Organometallics* **21**, 1982 (2002).
13. C. Z. Li, E. Widjaja, and M. Garland, *J. Catal.* **213**, 126 (2002).
14. E. Widjaja, C. Z. Li, W. Chew, and M. Garland, *Anal. Chem.* **75**, 4499 (2003).
15. E. Widjaja, N. J. Crane, T. C. Chen, M. D. Morris, M. A. Ignelzi, and B. R. McCreddie, *Appl. Spectrosc.* **57**, 1353 (2003).
16. C. A. Lieber and A. Mahadevan-Jansen, *Appl. Spectrosc.* **57**, 1363 (2003).
17. V. Tuchin, *Tissue Optics. Light Scattering Methods and Instruments for Medical Diagnosis* (SPIE Press, Bellingham, WA, 2000) pp. 3–108.